RSC Advances

ROYAL SOCIETY OF CHEMISTRY

www.rsc.org/advances

Effect of vacancies in monolayer MoS_2 on electronic properties of Mo-MoS_2 contacts

Li-ping Feng*, Jie Su, Zheng-tang Liu

State Key Lab of Solidification Processing, College of Materials Science and Engineering, Northwestern Polytechnical University, Xi'an, Shaanxi, 710072, People's Republic of China

Abstract: Revealing the influence of intrinsic defects in monolayer MoS_2 on electronic nature of metal-MoS_2 contacts is particularly critical for their practical use as nanoelectronic devices. This work presents a systematic study toward electronic properties of Mo metal contacts to monolayer MoS_2 with vacancies by using first-principles calculations based on density functional theory. Upon Mo- and S-vacancy forming in monolayer MoS_2, both height and width of the tunnel barrier between Mo metal and monolayer MoS_2 are decreased. Additionally, Schottky barrier of 0.1 eV for perfect Mo-MoS_2 top contact is reduced to zero for defective ones. Partial density of states near Fermi level of defective Mo-MoS_2 top contacts are strengthened and electron densities at the interface of defective Mo-MoS_2 top contacts are increased compared with those of perfect one, suggests Mo- and S-vacancy in monolayer MoS_2 have possibility to improve the electron injection efficiency. Mo-vacancy in monolayer MoS_2 is beneficial to get high quality *p*-type Mo-MoS_2 contact, whereas S-vacancy in monolayer MoS_2 is favorable to achieve high quality *n*-type Mo-MoS_2 contact. Our findings provide important insights into future designing and fabrication of nanoelectronic devices with monolayer MoS_2.

Keywords: Density functional theory; Monolayer MoS_2; Vacancy; Mo metal; Electronic properties

1. Introduction

Monolayer transition-metal dichalcogenides (mTMD), a family of 2D semiconductor layers

* Corresponding author. Tel.: +86 29 88488013; fax: +86 29 88492642.
E-mail: lpfeng@nwpu.edu.cn (Dr. L. P. FENG)

arranged in a hexagonal lattice, have been drawn tremendous attention as promising channel materials for digital electronic applications due to their nonzero band gap, small thicknesses, and pristine interfaces without out-of-plane dangling bonds [1-10]. Among various mTMD materials, monolayer MoS_2 has emerged because of its atomically thickness of ~7 Å/layer [11], considerable band gap of 1.8 eV [12], planar nature, and pristine surfaces. Most recently, monolayer MoS_2 has been used to construct field-effect transistors (FETs), which can offer lower power consumption than classical transistors [1, 13]. New phototransistor based on monolayer MoS_2 has been demonstrated to have a better photoresponsivity as compared with the graphene-based device [14]. Moreover, FET based biosensors with mTMD semiconductor as the channel material have been fabricated and exhibit highly advantageous over all other nanomaterial-based FET biosensors [15].

However, low-resistance metal contacts to monolayer MoS_2 remain a critical issue for its transistor applications because several factors, such as large band gap, pristine surfaces and lack of proper doping approach, may mask the innate exceptional electronic and magnetic properties of monolayer MoS_2 [16, 17]. In order to overcome this issue, many studies have been performed to reduce the tunnel barrier and Schottky barrier in metal-MoS_2 contacts [16-20]. Popov et al. [20] have studied Ti-MoS_2 and Au-MoS_2 top contacts by density functional theory, indicating that the most common contact Au metal is rather inefficient for electron injection into monolayer MoS_2. Kang et al. [16] have evaluated In, Ti, Au, Pd, and Mo, contacts to monolayer MoS_2 by density functional theory calculations, implying that Ti and Mo have great potential to form favorable *n*-type top contacts to monolayer MoS_2. Nevertheless, the Schottky barrier for Ti-MoS_2 contact is about 0.33 eV [17], which is still very high. Mo-MoS_2 contact has ultra-low Schottky barrier of 0.1 eV at source/drain-channel junction, and high-performance FETs based on Mo-MoS_2 contact have been demonstrated [17]. Hence, Mo has been proposed as a promising contact metal to monolayer

MoS_2.

Vacancy defects were found to exist in monolayer MoS_2 when monolayer MoS_2 was prepared through sonochemical deposition [21] and exfoliated method [22]. Several literatures have reported the effect of vacancies on properties of monolayer MoS_2. Ataca et al. [23, 24] have calculated the formation energy of neutral vacancies in monolayer MoS_2 and studied the influence of vacancies on magnetic properties of monolayer MoS_2, implying that vacancy creation appears to be a promising way to extend the applications of MoS_2. The formation energies of charged vacancies in monolayer MoS_2 under different atmospheric conditions have been investigated [25, 26]. Feng et al. [27] have indicated that structural, electronic, and optical properties of monolayer MoS_2 depend greatly on its intrinsic vacancies.

It should be noted that vacancy defects in monolayer MoS_2 not only influence the properties of monolayer MoS_2 but also affect the interfacial and electrical properties of metal-MoS_2 contacts. However, to the best of our knowledge, effects of vacancies in monolayer MoS_2 on electronic structure and electronic properties of Mo-MoS_2 contact are not well understood yet. It is well known that the knowledge of electronic properties of Mo-MoS_2 contact is very important for the practical applications of monolayer MoS_2 as well as for the designing and analyzing of optoelectronic devices. Therefore, this work is focused on investigating the effect of vacancies in monolayer MoS_2 on electronic structure and electronic properties of Mo-MoS_2 contacts using first-principles calculations.

2. Computational details

In the present calculations, the exchange correlation of the generalized gradient approximation (GGA) with the Perdew-Burke-Ernzerhof (PBE) functional as implemented in CASTEP code [28] was employed. In order to consider the van der Waals interactions in TMD

materials, DFT-D2 is adopted in this work, where the potential is described via a simple pairwise force field and is optimized for popular DFT functionals [29]. The electron-ion interactions were described by norm-conserving Troullier-Martins pseudopotentials [30] with partial core corrections. The plane-wave cutoff energy was set to be 200 Ry after extensive convergence analysis. The Brillouin-zone of Mo-MoS_2 top contact region was performed over the 8 × 8 × 1 *k*-point grids using the Monkorst-Pack method [31], where the self-consistent convergence of the total energy is 1.0 × 10^{-6} eV/atom. Conjugate gradient scheme was used to relax supercell until the component of the forces on each atom was less than 0.01 eV/Å.

Mo-MoS_2 top contact was modeled by a supercell slab, which is periodic in the *x* and *y* directions and separated by 20 Å vacuum region in the *z* direction to minimize the interactions between adjacent image cells. The supercell slab of Mo-MoS_2 top contact contains 4×4 unit cells of monolayer MoS_2 and the close-packed surfaces of Mo (001) extending to the 6th layer, which is the most probable orientation to be found in experiments. The supercell geometry of perfect Mo-MoS_2 top contact is shown in Fig. 1(a), and geometries of defective Mo-MoS_2 top contacts with single Mo and S vacancy are presented in Fig. 1(b) and (c), respectively. When optimizing these models by using conjugate gradient technique, atoms except the 3^{rd} to 6^{th} layers of Mo metal from the interface were allowed to relax so as to evaluate the effect of interfacial layers [17]. Although in real situations, the contact metals consist of many layers, the situation restricted to 6 layers of metal atoms is thick enough to accurately model the electronic properties of metal-MoS_2 contact [17, 20, 32] because the obtained results do not change appreciably beyond this thickness. A similar approach had been successfully used to characterize mTMD and their contacts to metal electrodes [20, 27].

3. Results and discussion

3.1 Tunnel barriers

The tunnel barrier between a metal and mTMD is characterized by its height and width, which are evaluated by the effective tunnel barrier height ($\Phi_{TB,eff}$) and physical separation (d_p), respectively. The $\Phi_{TB,eff}$ is defined as the minimum effective potential (V_{eff}) difference between the Mo-MoS_2 interface and monolayer MoS_2. According to Kohn-Sham equations [33] and Kang et al. [16] reports, the effective potential of an electron ($V_{eff}(n)$) represents the electron interaction with other electrons and external electrostatic field, and $V_{eff}(n)$ can be expressed by [16, 33]

$$V_{eff}(n)=V_{KS}=V_H(n)+V_{xc}(n)+V_{ext}(n) \quad (1)$$

where $V_H(n)$ is the mean-field electrostatic interaction, $V_{xc}(n)$ is the exchange-correlation potential, V_{ext} represents external electrostatic interactions, and V_{KS} is the Kohn-Sham potential in Kohn-Sham equations. Fig. 2(a), as an example, shows the V_{eff} versus position on z axis for perfect Mo-MoS_2 top contact and denotes the $\Phi_{TB,eff}$ of perfect Mo-MoS_2 top contact. To evaluate the tunnel barrier height, the $\Phi_{TB,eff}$ of perfect and defective Mo-MoS_2 top contacts are plotted in Fig. 2(b). Obviously, $\Phi_{TB,eff}$ value of perfect Mo-MoS_2 top contact is about 0.12 eV, which is lower than those of Ti-MoS_2 (0.45 eV [20]), Au-MoS_2 (1.03 eV [20]) and Pd-MoS_2 (0.15 eV [16, 32]) top contacts, implying that perfect Mo-MoS_2 top contact has higher carrier injection efficiency than Ti-, Au- and Pd-MoS_2 top contacts [16]. When a Mo- or S-vacancy is formed in monolayer MoS_2, defective Mo-MoS_2 top contacts have negligible $\Phi_{TB,eff}$ value of 0.01 eV, indicating that carrier injection efficiency of defective Mo-MoS_2 top contacts is further improved. It should be mentioned that these estimates of $\Phi_{TB,eff}$ can be affected by a sizeable Self-Interaction Error (SIE) [34-37], owing to the use of the non-SIE free PBE functional. The SIE can be estimated to contribute an additional 0.18-0.27 eV to the calculated barriers.

In order to evaluate the tunnel barrier width, physical separations of perfect and defective

Mo-MoS_2 contacts are calculated and presented in Fig. 2(b). The physical separation $d_{S\text{-}Mo}$ and average separation $d_{Mo\text{-}Mo}$ are defined as shown in Fig. 1(a). It is clear from Fig. 2(b) that $d_{S\text{-}Mo}$ value of perfect Mo-MoS_2 contact is about 1.34 Å, which is consistent with previous theoretical value (1.27 Å [16]) and smaller than those of other metal-MoS_2 top contacts (2-3 Å) [20, 32]. This small physical separation is lower than the sum of S and Mo covalent radii [20]. Furthermore, the average separation $d_{Mo\text{-}Mo}$ between the bottom Mo layer and the Mo layer in monolayer MoS_2 is about 3.02 Å, which is shorter than those of Ti-MoS_2 (3.57 Å) and Au-MoS_2 (4.21 Å) [20] top contacts. The small $d_{S\text{-}Mo}$ and $d_{Mo\text{-}Mo}$ indicate strong orbital overlaps and thin tunnel barrier.

When Mo-vacancy is formed in monolayer MoS_2, $d_{S\text{-}Mo}$ value of defective Mo-MoS_2 top contact is reduced to 1.29 Å as shown in Fig. 2(b). There are two factors may lead to the decrease of the $d_{S\text{-}Mo}$ value. On one hand, S ions surrounding Mo-vacancy undergo an outward relaxation [27]. On the other hand, dangling bonds of S ions, which induced by Mo-vacancy, can rebind with the Mo atoms in bottom Mo layer to shorten $d_{S\text{-}Mo}$. When S-vacancy is formed in monolayer MoS_2, $d_{S\text{-}Mo}$ value of defective Mo-MoS_2 top contact is decreased to 1.25 Å because the Mo atoms around S-vacancy move toward to the vacancy [27, 38]. Moreover, the average separation $d_{Mo\text{-}Mo}$ between the bottom Mo layer and the Mo layer in monolayer MoS_2 is reduced from 3.02 to 2.92 Å, which is close to the diameter of Mo atom. Therefore, compared with perfect Mo-MoS_2 contact, defective Mo-MoS_2 top contacts are favorable to get stronger orbital overlaps and thus thinner tunnel barrier.

3.2 Density of states

The band structure and PDOS of monolayer MoS_2 are shown in Fig. 3(a) and (b), respectively. It can be seen that an obvious band gap of 1.78 eV is observed for monolayer MoS_2, which is consistent with the theoretical values of 1.73 eV [39] and 1.90 eV [40] obtained using GGA, but lower than the values of 2.12-2.78 eV obtained by HSE06 [41, 42] and GW [23, 43] (see

Supplementary Table 1). The experimental value of 1.80 eV [12] may be rather an optical band gap because of the experimental methods used and the approximations applied in the treatment of the data. Hence, the band gap of monolayer MoS_2 obtained by the higher-level functionals of HSE06 [41, 42] and GW [23, 43] may be more close to the true experimental data. This is consistent with the expectation that the PBE Kohn-Sham gap usually underestimates the true band gap.

Fig. 3(c) presents the PDOS of perfect Mo-MoS_2 top contact. It is obvious from Fig. 3(c) that the band gap vanishes, indicating a metallic contact between Mo metal and monolayer MoS_2. According to the previous reports [16, 20], the *n*-type or *p*-type can be determined from the PDOS of monolayer MoS_2 in the Mo-MoS_2 contact. If the position of Fermi level (E_F) is shifted upwards the original conduction bands (E_c) of monolayer MoS_2, indicating that monolayer MoS_2 is doped *n* type. In contrast, if E_F is close to the original valence bands (E_v) of monolayer MoS_2, showing that monolayer MoS_2 is doped *p* type. In Fig. 3(c), the E_F of perfect Mo-MoS_2 top contact is shifted upwards, to 0.25 eV above the bottom of conduction bands of monolayer MoS_2, suggesting that monolayer MoS_2 is doped *n*-type by Mo. The shift of E_F is due to the fact that doping causes significant distortion to the band structure around the band gap. In order to comparatively study the PDOS of monolayer MoS_2 under different conditions, it is necessary to lineup the band structures of intrinsic monolayer MoS_2 and monolayer MoS_2 in Mo-MoS_2 top contacts. For this purpose, the valence bands maximum (E_{VBM}) of Mo-MoS_2 top contacts can be obtained by the following equation [44, 45]:

$$E_{VBM}=E_{VBM}(\text{intrinsic})+V_{av}(\text{interface})-V_{av}(\text{intrinsic}) \quad (1)$$

where E_{VBM}(intrinsic) is the valence bands maximum of intrinsic monolayer MoS_2, V_{av}(intrinsic) and V_{av}(interface) represent the average potential of intrinsic monolayer MoS_2 and monolayer MoS_2 in Mo-MoS_2 top contacts, respectively. As a result, the band structures of Mo-MoS_2 top contacts are

obtained (see Supplementary Figure 1). The borders of the valence and conduction bands of intrinsic monolayer MoS_2 are marked as vertical dot lines in the PDOS of Mo-MoS_2 top-contacts, as shown in Fig. 3(c). The dash line in Fig. 3(c) represents the E_F of the Mo-MoS_2 contact system. According to the previous reports [16, 46], the *n*-type (*p*-type) Schottky barrier is the difference between the bottom of conduction bands (the top of the valence bands) of intrinsic monolayer MoS_2 and the E_F of the Mo-MoS_2 top contact, as exhibited in Fig. 3(c). Like In-, Ti-, and Au-MoS_2 top contacts [16, 20, 47], the E_F is pinned near the original conduction bands of intrinsic monolayer MoS_2. The Schottky barrier of perfect Mo-MoS_2 top contact is about 0.1 eV, which is in good agreement with previous theoretical results (0.13 eV [16], 0.1 eV [17]) and lower than those of Ti-MoS_2 (0.33 eV [17, 32], 0.35 eV [16]), Au-MoS_2 (0.62 eV [16, 32]) and Pd-MoS_2 (0.90 eV [16, 32]) top contacts despite metal Mo has a high work function. In addition, high PDOS spread all over the original band gap of intrinsic monolayer MoS_2 implies the formation of Ohmic contact between Mo metal and monolayer MoS_2, which is consistent with previous theoretical and experimental report for Mo-MoS_2 top contact [17, 32]. Furthermore, the broadening of the peaks in the PDOS near E_F reflects the formation of delocalized states with low effective electron mass allowing more electrons to be transferred between the metal and the mTMD layer [20, 32].

PDOS of defective Mo-MoS_2 top contacts with single Mo and S vacancy are presented in Fig. 3(d) and (e), respectively. In the case of Mo-vacancy, as shown in Fig. 3(d), a high PDOS near E_F eliminates the band gap, indicating that Mo-vacancy has no effect on Ohmic contact and the metallic character of Mo-MoS_2 system. In addition, PDOS near E_F of defective Mo-MoS_2 top contact are much higher than those of perfect one because the dangling bonds of S atoms surrounding Mo-vacancy can form covalent bonding with Mo atoms in the bottom Mo layer, which almost like the covalent bonding formation for Mo-MoS_2 side contact [16]. The higher PDOS near

E_F suggests the lower effective carrier mass and the higher efficiency of carrier transport. Hence, upon Mo-vacancy forming in monolayer MoS_2, the Schottky barrier of defective Mo-MoS_2 top contact vanishes. Moreover, in contrast to perfect Mo-MoS_2 top contact, the E_F of defective Mo-MoS_2 top contact is shifted downwards, to 0.17 eV under the top of valence bands of monolayer MoS_2. Therefore, Mo-vacancy in monolayer MoS_2 is beneficial to achieve high quality *p*-type Mo-MoS_2 top contact.

In the case of S-vacancy, as shown in Fig. 3(e), high PDOS near E_F are also observed. Previous studies [27, 38] have shown that S-vacancy in monolayer MoS_2 can induce defective states in the band gap. Thus, it can be found that some new peaks of PDOS appear near E_F due to strong hybridization of *d* orbitals between Mo metal and monolayer MoS_2. Additionally, the Schottky barrier of defective Mo-MoS_2 top contact disappears, implying the efficiency of electron transport is further improved. Similar to perfect Mo-MoS_2 top contact, the E_F of defective Mo-MoS_2 top contact is shifted upwards, to 0.62 eV above the bottom of conduction bands of intrinsic monolayer MoS_2. It should be noted that the position of the E_F of defective Mo-MoS_2 top contact is higher than that of perfect one. Therefore, in contrast to Mo-vacancy, S-vacancy is beneficial to achieve high quality *n*-type Mo-MoS_2 top contact.

3.3 Electron density

Average electron density of perfect and defective Mo-MoS_2 top contacts are calculated and shown in Fig. 4. The minimum *x*-*y* plane average electron density of Mo-MoS_2 interface and monolayer MoS_2 is marked ρ_i and ρ_m, respectively. Usually, high electron density at the interface of metal-mTMD contacts allows sufficient injection of charge into mTMD layer [20]. In Fig. 4(a), the ρ_i value of perfect Mo-MoS_2 top contact is about 0.042 $bohr^{-3}$, which is higher than those of other metal-MoS_2 top contacts (0.013-0.033 $bohr^{-3}$) [16, 20], implying that Mo metal has advantage to

achieve strong orbital overlaps with monolayer MoS_2, leading to low contact resistant and high electron injection efficiency [32]. The previous studies [17, 27] have indicated that strong covalent bonds are formed at the interface of perfect Mo-MoS_2 top contact. From Fig. 4(a), the ρ_i value of 0.042 $bohr^{-3}$ is close to the ρ_m value of 0.051 $bohr^{-3}$, indicating the formation of covalent bonds at the interface. This result is consistent with the previous reports [17, 27].

Average electron densities of defective Mo-MoS_2 top contacts with single Mo and S vacancy are presented in Fig. 4(b) and (c), respectively. It can be seen that the average electron densities at the interface region of defective Mo-MoS_2 top contacts become higher compared with those in perfect Mo-MoS_2 system, showing that the covalent bonds between the Mo metal and monolayer MoS_2 are enhanced due to stronger orbital overlap, which are consistent with the above PDOS analysis. Consequently, Mo- and S-vacancy in monolayer MoS_2 have possibility to decrease the contact resistant and improve the electron injection efficiency. In addition, the ρ_i value of 0.047 $bohr^{-3}$ for Mo-MoS_2 top contact with S-vacancy is slightly larger than the ρ_i value of 0.044 $bohr^{-3}$ for Mo-MoS_2 top contact with Mo-vacancy, indicating that S-vacancy is more favorable to improve the electronic transport of Mo-MoS_2 top contacts. After introduction of Mo- or S-vacancy in monolayer MoS_2, the difference between ρ_i and ρ_m for defective Mo-MoS_2 top contacts is decreased.

3.4 Mulliken Population

The electron density can also be confirmed by Mulliken population analysis. The calculated Mulliken populations of atoms in Mo metal layer and monolayer MoS_2 for perfect and defective Mo-MoS_2 top contacts are listed in Table 1. For perfect Mo-MoS_2 top contact, 0.042 *e* of Mo atoms in metal layer are transferred to interfacial S atoms in top sulfur layer, suggesting strong interactions between the Mo and S atoms. Simultaneously, interfacial S atoms accept 0.079 *e* from Mo atoms in

monolayer MoS_2. As a result, the electron density at the Mo-MoS_2 interface region is lower than that of Mo-S bond in monolayer MoS_2. For defective Mo-MoS_2 top contacts, the electrons transferred from Mo atoms in metal layer to interfacial S atoms are increased whereas the electrons moved from Mo atoms in monolayer MoS_2 to interfacial S atoms are decreased compared with those in perfect Mo-MoS_2 top contact, as shown in Table 1. Accordingly, the electron density at the Mo-MoS_2 interface region increases whereas the electron density of Mo-S bond in monolayer MoS_2 reduces. Therefore, the difference between ρ_i and ρ_m for defective Mo-MoS_2 top contacts is decreased, which is consistent with above electron density analysis.

4. Conclusion

The effects of intrinsic vacancy in monolayer MoS_2 on electronic structure and electronic properties of Mo-MoS_2 top contacts have been investigated using the first-principles plane-wave pseudopotential method based on density functional theory. Tunnel barrier, Schottky barrier, and electron density of perfect and defective Mo-MoS_2 top contacts were analyzed. Results show that the height and width of the tunnel barrier of Mo-MoS_2 top contacts are decreased when Mo- or S-vacancy is formed in monolayer MoS_2. Additionally, Schottky barriers are found to be 0.1 and 0 eV for perfect and defective Mo-MoS_2 top contacts, respectively. PDOS near Fermi level of defective Mo-MoS_2 top contacts are much higher than those of perfect one, implying the lower effective carrier mass for defective Mo-MoS_2 top contacts. Average electron density at interface of defective Mo-MoS_2 top contacts are increased compared with those in perfect Mo-MoS_2 top contact, showing that contact resistant and electron injection efficiency are further improved by vacancies. Moreover, Mo-vacancy in monolayer MoS_2 exhibits *p*-type Mo-MoS_2 top contact, whereas S-vacancy in monolayer MoS_2 shows *n*-type Mo-MoS_2 top contact.

Acknowledgments

We acknowledge the National Natural Science Foundation of China under grant No. 61376091, the National Aerospace Science Foundation of China under grant No. 2014ZF53070, the Fundamental Research Funds for the Central Universities under grant No. 3102014JCQ01033 and the 111 Project under grant No. B08040.

References

[1] B. Radisavljevic, A. Radenovic, J. Brivio, V. Giacometti, A. Kis, *Nat. Nanotechnol*. 2011, **6**, 147.

[2] H. S. Song, S. L. Li, L. Gao, Y. Xu, K. Ueno, J. Tang, et al. *Nanoscale*, 2013, **5**, 9666.

[3] B. Radisavljevic, M. B. Whitwick, A. Kis, *App. Phys. Lett*. 2012, **101**, 043103.

[4] H. Fang, S. Chuang, T. C. Chang, K. Takei, T. Takahashi, A. Javey, *Nano Lett*. 2012, **12**, 3788.

[5] J. Khan, C. M. Nolen, D. Teweldebrhan, D. Wickramaratne, R. K. Lake, A. A. Balandin, *App. Phys. Lett*. 2012, **100**, 043109.

[6] J. Mann, Q. Ma, P. M. Odenthal, M. Isarraaraz, D. Le, E. Preciado, et al. *Adv. Mater*. 2014, **26**, 1399.

[7] W. S. Hwang, M. Remskar, R. Yan, V. Protasenko, K. Tahy, S. D. Chae, et al. A. *App. Phys. Lett*. 2012, **101**, 013107.

[8] J. W. Jiang. *Nanoscale* 2014, **6**, 8326.

[9] X. Liu, M. I. B. Utama, J. Lin, X. Gong, J. Zhang, Y. Zhao, *Nano Lett*. 2014, **14**, 2419.

[10] Q. H. Wang, K. Kalantar-Zadeh, A. Kis, J. N. Coleman, M. S. Strano, *Nat. Nanotechnol.* 2012, **7**, 699.

[11] M. M. Benameur, B. Radisavljevic, J. S. Heron, H. Berger, A. Kis, *Nanotechnol.* 2011, **22**, 125706.

[12] K. F. Mak, C. Lee, J. Hone, J. Shan, T. F. Heinz, *Phys. Rev. Lett*. 2010, **105**, 136805.

[13] W. Bao, X. Cai, D. Kim, K. Sridhara, M. S. Fuhrer, *Appl. Phys. Lett*. 2013, **102**, 042104.

[14] Z. Yin, H. Li, H. Li, L. Jiang, Y. Shi, Y. Sun, et al. *ACS Nano* 2012, **6**, 74.

[15] D. Sarkar, W. Liu, X. Xie, A. Anselmo, S. Mitragotri, K. Banerjee, *ACS Nano* 2014, **8**, 3992.

[16] J. Kang, W. Liu, D. Sarkar, D. Jena, K. Banerjee, *Phys. Rev. X* 2014, **4**, 031005.

[17] J. Kang, W. Liu, K. Banerjee, *Appl. Phys. Lett*. 2014, **104**, 093106.

[18] S. Das, H. Y. Chen, A. V. Penumatcha, J. Appenzeller, *Nano Lett*. 2013, **13**, 100.

[19] C. Gong, C. Huang, J. Miller, L. Cheng, Y. Hao, D. Cobden, et al. *ACS Nano* 2013, **7**, 11350.

[20] I. Popov, G. Seifert, D. Tománek, *Phys. Rev. Lett*. 2012, **108**, 156802.

[21] N. A. Dhas, K. S. Suslick, *J. Am. Chem. Soc*. 2005, **127**, 2368.

[22] S. McDonnell, R. Addou, C. Buie, R. M. Wallace, C. L. Hinkle, *ACS Nano* 2014, **8**, 2880.

[23] C. Ataca, S. Ciraci, *J. Phys. Chem. C* 2011, **115**, 13303.

[24] C. Ataca, H. Sahin, E. Akturk, S. Ciraci, *J. Phys. Chem. C* 2011, **115**, 3934.

[25] L. P. Feng, J. Su, S. Chen, Z. T. Liu, *Mater. Chem. Phys*. 2014, **148**, 5.

[26] D. Liu, Y. Guo, L. Fang, J. Robertson, *Appl. Phys. Lett.* 2013, **103**, 183113.

[27] L. P. Feng, J. Su, Z. T. Liu, *J. Alloy Compd.* 2014, **613**, 122.

[28] M. D. Segall, P. J. D. Lindan, M. J. Probert, C. J. Pickard, P. J. Hasnip, S. J. Clark, M. C. Payne, *J. Phys.: Condens. Matter.* 2002, **14**, 2717.

[29] T. Bučko, J. Hafner, S. Lebègue, and J. G. Ángyán. *J. Phys. Chem. A* 2010, **114**, 11814.

[30] N. Troullier, J. L. Martins, *Phys. Rev. B* 1991, **43**, 1993.

[31] H. J. Monkhorst, J. D. Pack, *Phys. Rev. B* 1976, **13**, 5188.

[32] J. Kang, D. Sarkar, W. Liu, D. Jena, K. Banerjee, *IEEE International Electron Devices Meeting*. 2012, pp, 407-410.

[33] W. Kohn, L. J. Sham, *Physical Review*. 1965, **140**, A1133.

[34] J. Robertson, K. Xiong, and S. J. Clark, *Thin Solid Films* 2006, **496**, 1-7.

[35] J. J. Liu, X. L. Fu, S. F. Chen, and Y. F. Zhu, *Appl. Phys. Lett.*, 2011, **99**, 191903.

[36] R. Gillen, and J. Robertson, Phys. *Revs. B* 2011, **84**, 035125.

[37] W. Li, C. F. J. Walther, A. Kuc, and T. Heine, *J. Chem. Theory Comput.* 2013, **9**, 2950-2958.

[38] W. Zhou, X. Zou, S. Najmaei, Z. Liu, Y. Shi, J. Kong, et al. *Nano Lett.* 2013, **13**, 2615.

[39] S. Lebègue, O. Eriksson, *Phys. Rev. B* 2009, **79**, 115409.

[40] A. Kumar, P. K. Ahluwalia, *Springer International Publishing*, 2014, **21**, 53.

[41] Y. Jing, X. Tan, Z. Zhou, P. Shen, *J. Mater. Chem. A* 2014, **2**, 16892.

[42] A. Kumar, P. K. Ahluwalia, *Physica B*. 2013, **419**, 66-75.

[43] Q. Yue, J. Kang, Z. Shao, X. Zhang, S. Chang, G. Wang, *Phys. Lett. A* 2012, **376**, 1166.

[44] A. Garcia, and J. E. Northrup, *Phys. Rev. Lett*. 1995, **74**, 1131.

[45] S. Poykko, M. J. Puska, and R. M. Nieminen, *Phys. Rev. B* 1996, **53**, 3813.

[46] M. Bokdam, G. Brocks, M. I. Katsnelson, and P. J. Kelly. arXiv preprint arXiv:1401.6440, 2014.

[47] W. Liu, J. Kang, D. Sarkar, Y. Khatami, D. Jena, K. Banerjee, *Nano Lett.* 2013, **13**, 1983.

Figure and table captions list:

Fig. 1 The supercell geometry of Mo-MoS_2 top contacts. (a) Bottom view and side view of perfect Mo-MoS_2 top contact, (b) Bottom view of defective Mo-MoS_2 top contact with Mo vacancy in monolayer MoS_2 and amplified sketch of monolayer MoS_2 with Mo vacancy, and (c) Bottom view of defective Mo-MoS_2 top contact with S vacancy in monolayer MoS_2 and amplified sketch of monolayer MoS_2 with S vacancy.

Fig. 2 (a) Minimum effective potential height (V_{eff}) versus z position for perfect Mo-MoS_2 top contact. The effective tunnel barrier height ($\Phi_{TB,eff}$) can be defined as the V_{eff} difference between the Mo-MoS_2 interface and monolayer MoS_2. Color key is Mo metal=blue and monolayer MoS_2=green. (b) The $\Phi_{TB,eff}$ and physical separation d_p for perfect and defective Mo-MoS_2 top contacts.

Fig. 3 (a) Band structure of intrinsic monolayer MoS_2, (b) PDOS of intrinsic monolayer MoS_2, (c) PDOS of perfect Mo-MoS_2 top contact, (d) PDOS of defective Mo-MoS_2 top contact with Mo-vacancy in monolayer MoS_2, (e) PDOS of defective Mo-MoS_2 top contact with S-vacancy in monolayer MoS_2.

Fig. 4 Average electron density value in the x-y planes normal to the z axis: (a) perfect Mo-MoS_2 top contact, (b) defective Mo-MoS_2 top contact with Mo-vacancy, (c) defective Mo-MoS_2 top contact with S-vacancy. Ball with a virtual edge in the panels represents Mo- or S-vacancy in monolayer MoS_2. The ρ_i and ρ_m in each panel indicate the minimum x-y plane average electron density at interface and monolayer MoS_2, respectively (in units of $bohr^{-3}$).

Table 1 Mulliken population of Mo atoms in metal layer as well as Mulliken population of Mo and S atoms in monolayer MoS_2 for perfect and defective Mo-MoS_2 top contacts. The atoms' serial number is indexed in Fig. 1 (b) and (c).

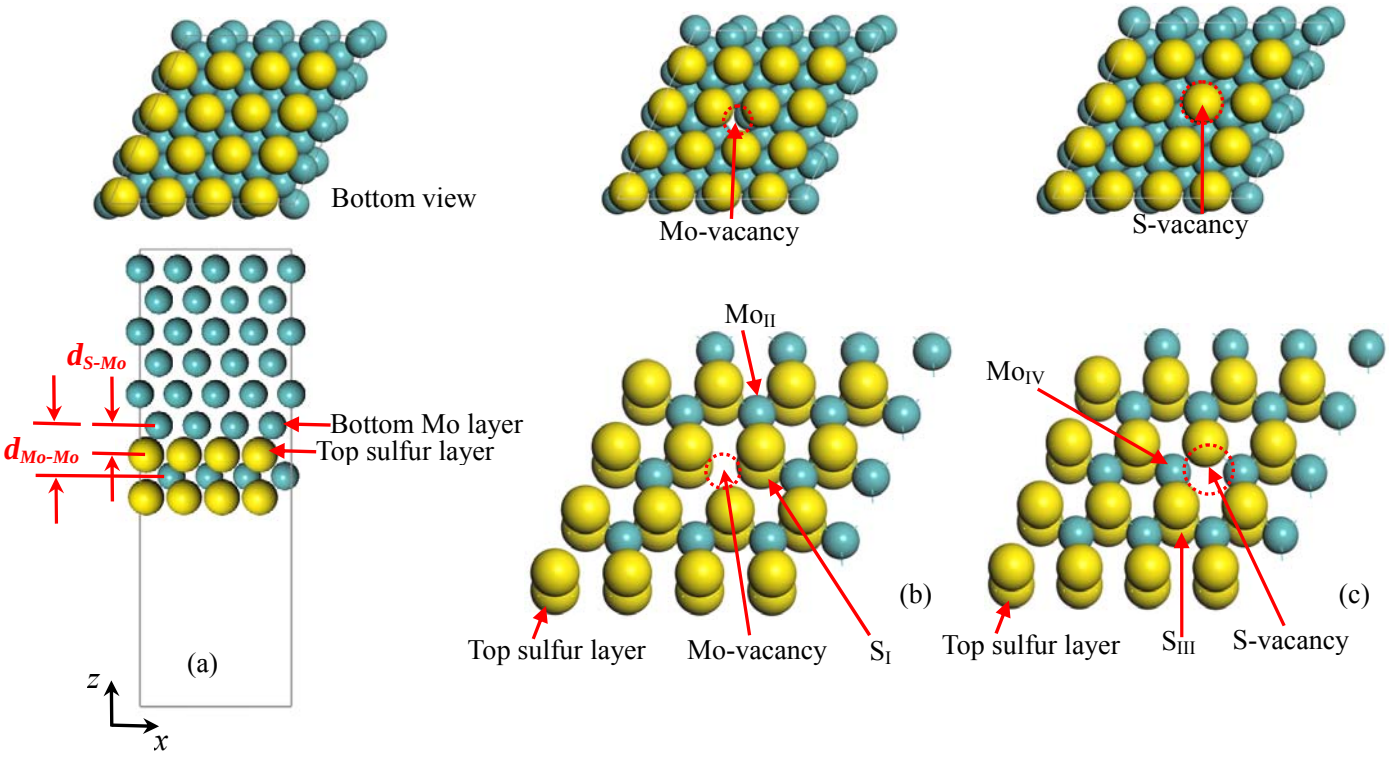

Fig. 1 The optimized geometry of Mo-MoS_2 top contacts. (a) Bottom view and side view of perfect Mo-MoS_2 top contact, (b) Bottom view of defective Mo-MoS_2 top contact with Mo vacancy in monolayer MoS_2 and amplified sketch of monolayer MoS_2 with Mo vacancy, and (c) Bottom view of defective Mo-MoS_2 top contact with S vacancy in monolayer MoS_2 and amplified sketch of monolayer MoS_2 with S vacancy.

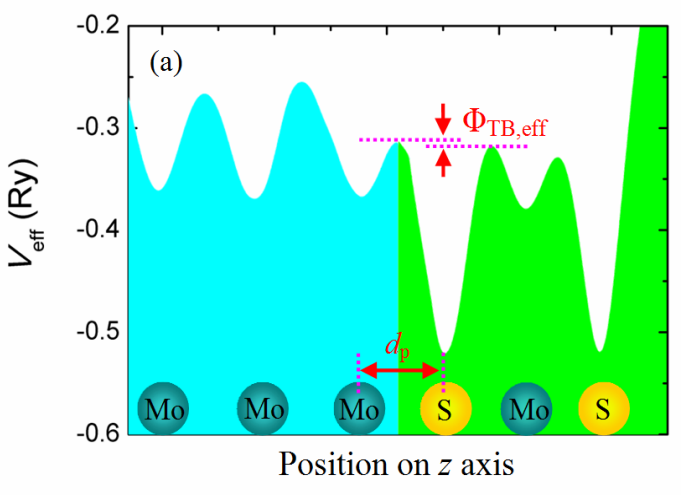

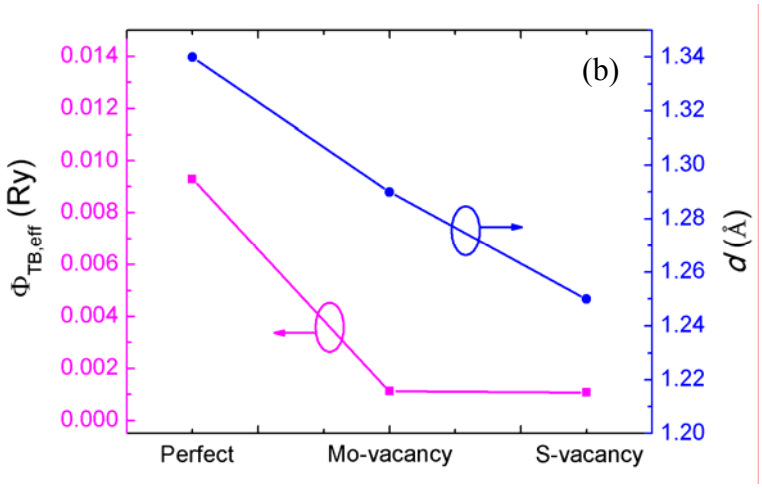

Fig. 2 (a) Minimum effective potential height (V_{eff}) versus z position for perfect Mo-MoS_2 top contact. The effective tunnel barrier height ($\Phi_{TB,eff}$) can be defined as the V_{eff} difference between the Mo-MoS_2 interface and monolayer MoS_2. Color key is Mo metal=blue and monolayer MoS_2=green. (b) The $\Phi_{TB,eff}$ and physical separation d_p for perfect and defective Mo-MoS_2 top contacts.

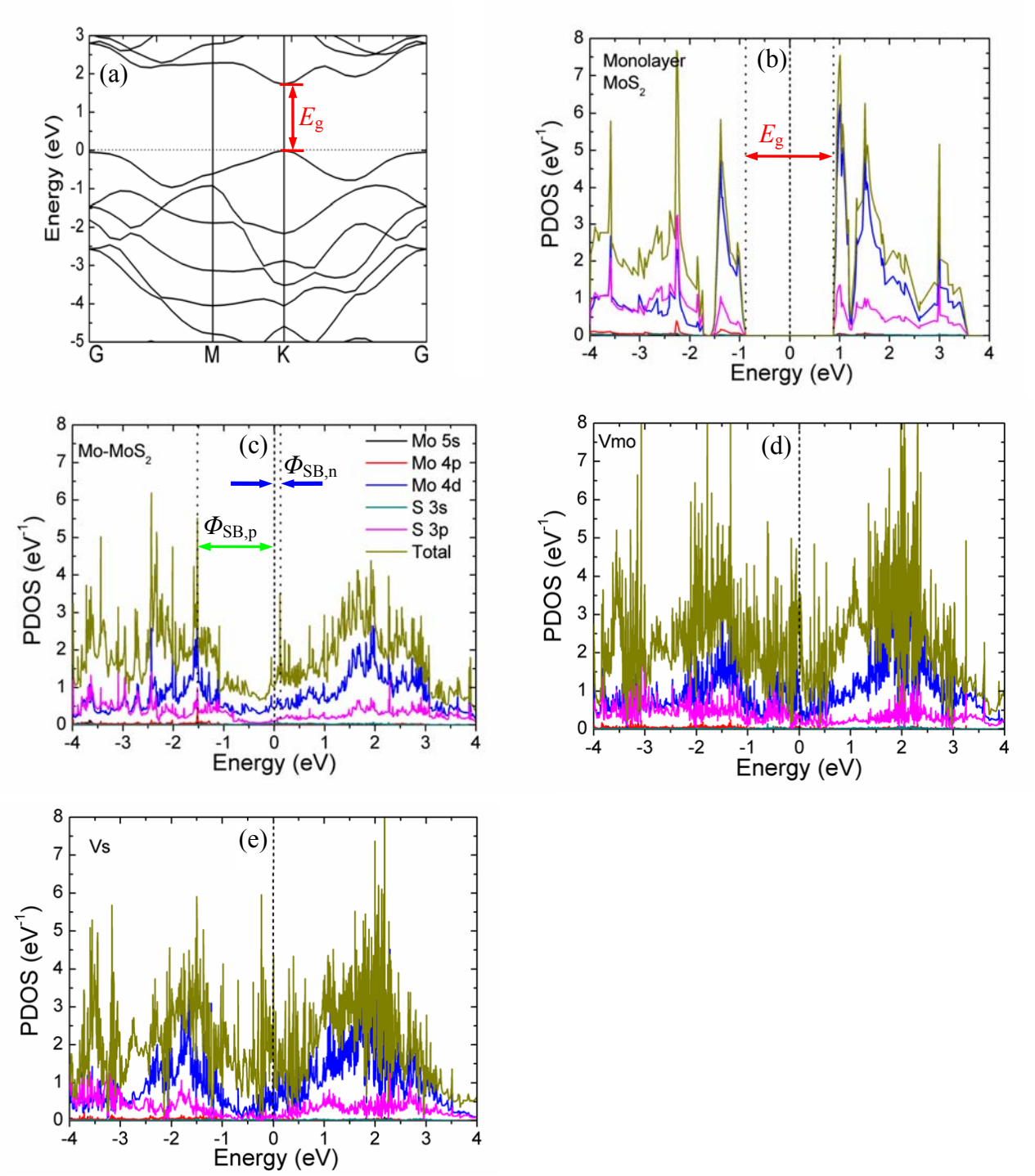

Fig. 3 (a) Band structure of intrinsic monolayer MoS_2, (b) PDOS of intrinsic monolayer MoS_2, (c) PDOS of perfect Mo-MoS_2 top contact, (d) PDOS of defective Mo-MoS_2 top contact with Mo-vacancy in monolayer MoS_2, (e) PDOS of defective Mo-MoS_2 top contact with S-vacancy in monolayer MoS_2.

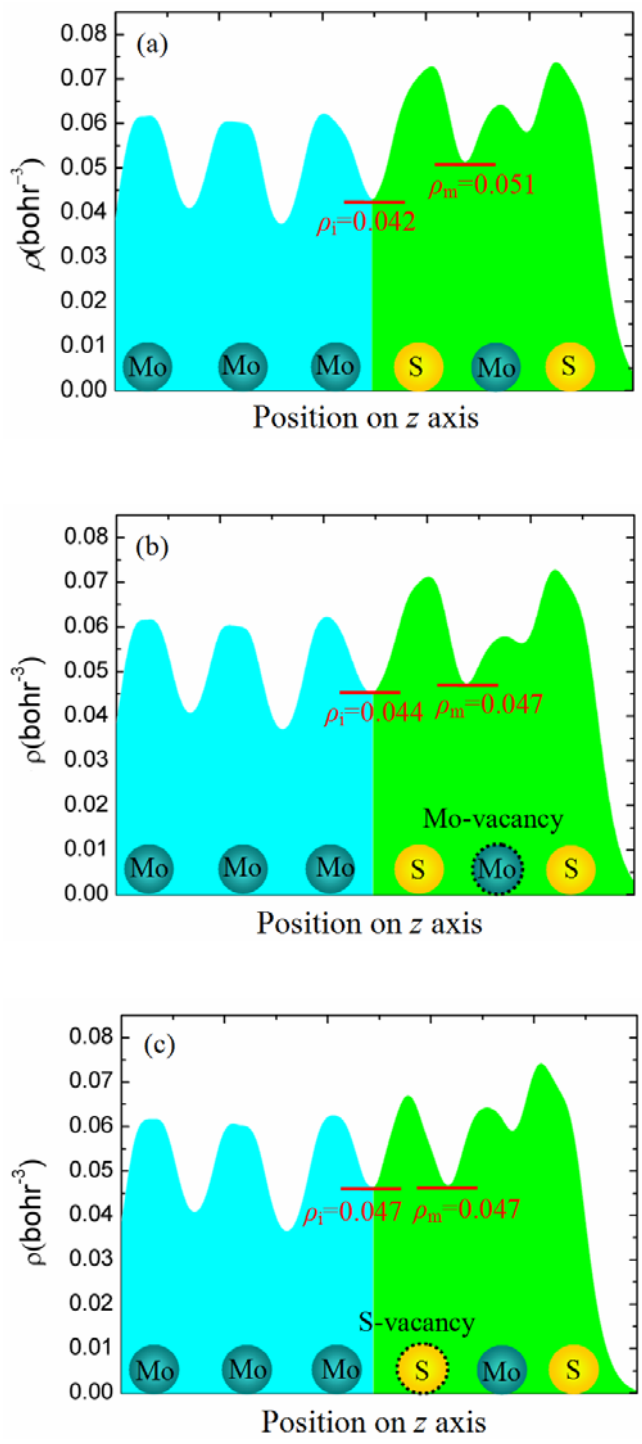

Fig. 4 Average electron density value in the *x*-*y* planes normal to the *z* axis: (a) perfect Mo-MoS_2 top contact, (b) defective Mo-MoS_2 top contact with Mo-vacancy, (c) defective Mo-MoS_2 top contact with S-vacancy. Ball with a virtual edge in the panels represents Mo- or S-vacancy in monolayer MoS_2. ρ_i and ρ_m in each panel indicate the minimum *x*-*y* plane average electron density at interface and monolayer MoS_2, respectively (in units of $bohr^{-3}$).

Table 1 Mulliken population of Mo atoms in metal layer as well as Mulliken population of Mo and S atoms in monolayer MoS_2 for perfect and defective Mo-MoS_2 top contacts. The atoms' serial number is indexed in Fig. 1 (b) and (c).

	Mo metal layer	Mo_{II}	Mo_{IV}	S_I	S_{III}
perfect	5.958	5.921	5.921	6.073	6.073
Mo-vacancy	5.946	5.940	-	6.082	-
S-vacancy	5.943	-	5.941	-	6.119

Title: Effect of Vacancies in Monolayer MoS_2 on Electronic Properties of Mo-MoS_2 Contacts

Authors: Li-ping Feng, Jie Su; Zheng-tang Liu